

RSC Advances



This is an *Accepted Manuscript*, which has been through the Royal Society of Chemistry peer review process and has been accepted for publication.

Accepted Manuscripts are published online shortly after acceptance, before technical editing, formatting and proof reading. Using this free service, authors can make their results available to the community, in citable form, before we publish the edited article. This *Accepted Manuscript* will be replaced by the edited, formatted and paginated article as soon as this is available.

You can find more information about *Accepted Manuscripts* in the [Information for Authors](#).

Please note that technical editing may introduce minor changes to the text and/or graphics, which may alter content. The journal's standard [Terms & Conditions](#) and the [Ethical guidelines](#) still apply. In no event shall the Royal Society of Chemistry be held responsible for any errors or omissions in this *Accepted Manuscript* or any consequences arising from the use of any information it contains.

SECOND ORDER HYPERPOLARIZABILITY OF TRIPHENYLAMINE BASED ORGANIC SENSITIZERS: A FIRST PRINCIPLE THEORETICAL STUDY

M. Prakasam^{a,b} and P. M. Anbarasan^{a,b*}

^aDepartment of Physics, Periyar University, Salem - 636 011, Tamil Nadu, India.

^bCentre for Nanoscience and Nanotechnology, Periyar University, Salem - 636 011, Tamil Nadu, India.

Abstract

The designed metal-free dyes have investigated by Density Functional Theory (DFT) and Time-Dependent - DFT (TD-DFT) to evaluate ground state and excited state geometries of triphenylamine-based organic sensitizers. Optoelectronic properties of five types of Triphenylamine (TPA) - based dyes, namely C206, TPA, TPA-N(CH₃)₂, TPA-SCH₃, TPA-OC₂H₅ were studied. Energy band modulation has been performed by these dyes with different electron donating and same electron withdrawing group. The performance of the hybrid functional B3LYP and wB97XD using a standard basis set 6-311++G(d,p) has been analyzed. Solvent effects have been examined by Conductor-like Polarizable Continuum Model (C-PCM) formalisms. The C-PCM/ TD-DFT results show that the accurate absorption energies have obtained only when solvent effect included in the excited state geometries. The theoretical examination on non-linear optical (NLO) properties was performed on the key parameters of static polarizability, first order and second order hyperpolarizability. A good photovoltaic performance based on the optimized geometry, the relative position of the frontier molecular orbital energy levels and the absorption maximum of the dye were proposed for offering a remarkable response. The results provide a direction for optimizing the dyes as efficient sensitizers in Dye Sensitized Solar Cells (DSSCs) and NLO applications.

Keywords: *Triphenylamine, Dye Sensitizer, DFT, Second Order Hyperpolarizability, UV-Visible Absorption Spectra.*

Corresponding Author:

P. M. Anbarasan (e-mail: profpmanbarasan@gmail.com)

Tel:+91 427 2345766, 2345520

Fax: +91 427 2345124, 2345565

Mobile: +91 9443659435

1. Introduction

Dye-sensitized solar cells (DSSCs) have more attractive and considerable attention in recent years as they offer the photo to electrical energy conversion at low-cost and thus they have been regarded as the next generation photovoltaic's cell [1, 2]. The dye, basically two types exist: First one metal-based dye-sensitized and another one is a metal free dye sensitizer. Although ruthenium-metal based sensitizer [3-5] offers an overall light energy to electrical energy conversion efficiency over 13.5%, the limited resources and the environmental issues relating to ruthenium use make it necessary to look after the alternative new dyes. In this regard, organic contains dyes have received much attention due to their environmentally friendly, low cost for device production and easy preparation process [6-12]. Other major advantages of these metal-free, dye sensitizer are their tunable absorption and photochemical properties through suitable molecular design [13, 14].

Among the DSSCs, the Bulk Hetero Junction model (BHJ) [15-17] is the most successful one. A DSSC is composed of four components namely transparent conducting oxide, counter-conducting electrodes, wide band-gap semiconductor surface, a dye molecule as sensitizer and an electrolyte using redox couple [18]. The working principle of DSSC involves photoexcitation of dye molecule thereby generation of an electron-hole pair. In the subsequent step upon absorption of light, the dye generates an exciton; the excited electron is injected into the conduction band of the TiO_2 ; the dye is regenerates the hole-transporting material (HTM), and the charges percolate to the electrodes. Two common back-reaction processes in DSSCs are observed: recombination of the electrons in the TiO_2 with the holes in the HTM and finally reduction of the oxidized dye. In this regard, TiO_2 is the mostly used semiconducting surface the conductance band of which is located at 4.0 eV [19-22].

From this energetic point of view, the most crucial steps of a photovoltaic cell are the injection and regeneration process. The following criteria to facilitate in these two processes: (i) The Lowest Unoccupied Molecular Orbital (LUMO) energy level of the dye molecule must lie above conduction band of the semiconductor materials (E_{CB}). (ii) The Highest Occupied Molecular Orbital (HOMO) of the dye molecules must be at lower energy than the chemical potential of the redox couple [23, 24]. During this whole electronic dynamic process, the electron injection efficiency to the CB of the semiconductor surface and the electron collection efficiency at the transparent conductive oxide electrode directly determine the short-circuit current density (J_{SC}) of DSSC. The potential difference between the Fermi level of electrons in the semiconductor substrate and the redox potential of the electrolyte

gives the open circuit photovoltage (V_{OC}). These two parameters are important factors determining the efficiency of DSSCs, as [25]

$$\eta = \frac{J_{sc} V_{oc} FF}{P_{IN}} \quad (1)$$

Where, FF is the fill factor at which DSSC operates with the maximum power point, which is mainly related to the total series of the resistance in the DSSC. P_{IN} is the input power of incident solar light. However, it should be pointed out the overall efficiency of DSSC also depends on some other parameters like recombination, etc. Obviously, an embedded dye over a metal oxide plays a key role in the energy conversion efficiency of a DSSC. Generally, metal-free organic dye sensitizers are constituted by donor group (D), π -bridge (π), and acceptor (A) moieties, so called D- π -A structure. This push-pull structure can induce the intramolecular charge transfer (ICT) from A to D through the π -conjugated molecules when the dye is irradiated to sunlight. This is important for harvesting the solar energy.

In order to act as an efficient dye sensitizer in the BHJ cell, it must have the following characteristics: there are (i) the dye must show broad absorption spectra covering whole UV and visible region to absorb maximum energy incoming from sunlight, (ii) it should have a low band gap, (iii) it should be able to prevent electron-hole recombination effectively, (iv) the dye should have high oscillator strength, (v) open circuit voltage of the dye must be very high, (vi) HOMO of the dye must lie below the redox couple and LUMO of the dye must lie above the conduction band (CB) of the semiconductor of the downhill movement of electron and uphill movement of hole and (vii) a good acceptor group must be added to the dye molecule to anchor well on the semiconductor surface. As the electronic energy levels of an organic dye molecule are tunable by varying donor-acceptor moieties, it is possible to design a dye with desired energy levels. An enormous effort has being taken for this purpose during the last couple of years [16, 26, 27].

One of the interesting topics nowadays organic photovoltaic's in past twenty-five years is to design, synthesis of low band-gap semiconducting materials, dye sensitizers and HTM for the use in the DSSCs [28, 29]. Triphenylamine (TPA) is one such kind of molecule, well and the excellent electron donating power and its huge steric hindrance give it the ability to prevent undesired dye aggregation with the semiconductor surface [30-34]. The dyes composed of TPA as a donor and cyanoacrylic acid/thiophene as acceptor/linker is of mammoth interest in recent time [35-38]. In this work, the following functional groups like

$\text{N}(\text{CH}_3)_2$, SCH_3 and OC_2H_5 have substituted in the TPA molecules and also compared the substitution with C206 dye molecules. Fig. 1. Shows the chemical structure of TPA based dye sensitizers. So, it incorporated both electron-rich and electron-deficient moieties into TPA unit. The aim is to photovoltaic parameters are tuned on substitution, as well as to find out the optimum dye system within the selected dyes. Based on this molecular design, more efficient dyes with higher V_{OC} and the least J_{SC} are compared with that of C206 dye.

2. Model and Computation Details

All the calculations were performed using Gaussian 09w [39] program. The geometries of the design dye molecules in the gas phase were optimized in ground state geometries via Density Functional Theory (DFT) [40] with B3LYP [41] hybrid functional and wB97XD [42] with the 6-311++G(d,p) basis set. The more deviation in estimating LUMO energy is well assigned in DFT due to weak correlation effect. The design the molecules are optimized at minimum energy and no imaginary frequency.

The excited state geometries were carried out by time-dependent DFT (TD-DFT) calculations to determine at 20 vertical excitations to the excited state of the molecules. Although more time consuming, the use of range separated DFT functional is a good way to treat this problem. Based on the optimized molecular structures of the dyes, we simulated the UV-Visible spectra of all of them in gas phase and solvent medium with B3LYP hybrid function using standard basis set. The DFT functional B3LYP contains no empirical parameters and reported to reproduce good electronic properties in the gas phase as well as a solvent medium within reasonable computational resources [43]. In a solvent medium in chloroform, the computations were performed by applying C-PCM using the integral equation formalism variant to describe the electrostatic solute-solvent interactions by the creation of solute cavity via a set of overlapping spheres [44]. The absorption spectra were spin-allowed in 20 singlet transitions.

3. Results and Discussion

3.1 The Electron-Donating Capacity of Modified Donor Groups

Mainly four types of dyes, which originated from the C206 were chosen to modified donor portion in Triphenylamine (TPA) as the donor portion in $\text{N}(\text{CH}_3)_2$, SCH_3 and OC_2H_5 . Subsequent addition of various donors, group differs the dyes viz TPA- $\text{N}(\text{CH}_3)_2$, TPA- SCH_3 and TPA- OC_2H_5 respectively. The optimized geometries of the dyes were shown in Fig. 2. To

anchor the proposed dyes molecules onto the semiconductor anatase surface, however, an anchoring group namely cyanoacrylic acid, has been attached to each the dye molecules at the acceptor portion. Table 1 shows that the geometric parameters especially selected some dihedral angles to design the dye molecules. It is expected that an efficient dye should maintain the co-planarity between the anchoring group to donor portion and the bridging unit to facilitate the electron transfer process from the donor portion to the semiconductor surface. It is revealed that the dyes TPA-N(CH₃)₂ and TPA are more coplanar than C206 indicating for better electron delocalization and intramolecular charge transfer. Co-planarity facilitates the recombination process, which in turns decreases the efficiency of the dye molecules as a photovoltaic material. Therefore, it requires a balance between charge transfer and electron recombination process.

To get further result insight into the molecular structure and electronic distribution of these dye molecules using molecular orbital analysis (MOA) have been performed. In this way, occupied and unoccupied molecular orbital's are of particular interest. Since they might be involved in the electron Charge Transfer (CT) process. During photoexcitation, one electron of the HOMO of the dye is transferred to the LUMO, which thereafter participate in the subsequent energy injection processes. Fig. 3, Indicates frontier molecular orbital's of the electron density distribution of the dyes. It is clear from that the HOMO of the dye molecules is more concentrated over the donor portion of the TPA moiety. The adjacent π -spacer (thiophene) in the LUMOs is more concentrated over the entire acceptor portion group. The situation becomes more prominent view that some electron-withdrawing groups are attached to the donor moiety. A spatial separation between the electron densities within the dye molecule and charge transfer process from dye to semiconductor surface through photoexcitation facilitation to be an efficient dye useful for DSSC.

It is evident that the dyes N(CH₃)₂ and TPA with spatial separation are more prominent and consequently expected to perform in a better way of selected dyes. The energy gaps (Δ) of the dye were optimized in B3LYP and wB97XD method, the optical band of dyes depicted in Table 2. It shows that TPA-N(CH₃)₂ and TPA dyes have Δ values in the order of 2 eV, whereas the dye TPA had much higher in the order of 0.15 eV. However, as also indicated by the energy positions of the HOMO and LUMO of the dyes, we expect to type-II band alignment in most of the cases, while attaching the dyes with TiO₂ semiconductor surface, keeping in the mind that, in the composite system, the quasi-particle energy levels are tunable depending upon the nature of dye molecules-adsorbent interaction [45]. It is

noteworthy to mention here that the use of TiO_2 semiconductor surface as a link of photoelectron in a solar cell is tested and is of crucial interest in recent days and we use TiO_2 surface referring the value of $E_{\text{CB}} = 4.0$ eV as reported [20]. Note that, the band bending as evident from the recent studies [45, 46] may alter the conduction band edge of TiO_2 surface which has a direct influence on the performance of a DSSC, although a very recent experiment demonstrates the higher photocatalytic activity of anatase surface of TiO_2 under flat-band condition [47].

3.2 Effects of Chemical Modifications

The electron injection process dye molecules and hence efficiency of dye in DSSC are governed by the energy levels of the dye with respect to the conduction band of the semiconductor surface. Interestingly, the most prominent feature of the organic dye is the tenability of these energy levels by introducing various functional groups, especially of the donor portion. For this purpose, we choose five different electron donating groups namely, TPA- $\text{N}(\text{CH}_3)_2$, TPA- SCH_3 , TPA- OC_2H_5 . The unsubstituted dyes are named as C206 and TPA respectively. It is worthy to mention here that all the groups are introduced at the donor part, firstly because the introduction of electron donating groups at the π -spacer increases steric repulsion and secondly the electron-withdrawing group at the π -spacer induces a negative effect on the DSSC's efficiency [48]. In this regard, electron-withdrawing groups on the π -spacer suppress the electron injection from the LUMO level to the semiconductor of the conduction band. Table 2 depicts how the electronic energy levels of the dyes are changed because substituent of the different functional groups. The HOMO and LUMO energy levels of the dyes (B3LYP method) C206, TPA- SCH_3 and TPA- $\text{N}(\text{CH}_3)_2$, are -5.30, -5.19, -5.10 eV and -2.88, -2.94, -3.20 eV, respectively. These values indicate that HOMO energy in dye TPA- $\text{N}(\text{CH}_3)_2$ is significantly lower due to the presence of the C206 group. In TPA- $\text{N}(\text{CH}_3)_2$ the LUMO level is greatly stabilized due to the highly electron withdrawing group, which is reflected by the low band gap 2.0 eV of C206. Now, concerning the effect of substituent's on the donor portion of the dyes it is revealed that attaching - $\text{N}(\text{CH}_3)_2$ and SCH_3 groups on the triphenylamine, it stabilizes both the HOMOs and LUMOs of TPA. The substituent - $\text{N}(\text{CH}_3)_2$ offers very low band gap in TPA- $\text{N}(\text{CH}_3)_2$ (2.0 eV) but for which the HOMO energy level is situated slightly higher than the reduction potential energy of the I_3^-/I^- electrolyte (-4.80 eV). The - OC_2H_5 group destabilizes the HOMO energy and reduces the

band gap to 3.19 in the dye C206. The HOMO and LUMO energy levels of all the TPA- N(CH₃)₂ dyes fulfill the requirements of a good sensitizer.

3.3 Electron Transfer and Photovoltaic Process

As already mentioned, suitable energy band is necessary to design molecules are desired photovoltaic performance. Thermodynamically, for the spontaneous electron charge transfer process from the excited state of the dye molecule to conduction band of TiO₂ requires LUMO energy of the dye to be at more positive potential than conduction band of TiO₂ (-4.0 eV) while HOMO energy values of the dyes should be more negative than reduction potential energy of the I₃⁻/I⁻ electrolyte (-4.80 eV). As displayed in Table 2, chemical modification of the substitution to the dye molecule changes the relative position of the frontier energy levels in a substantial amount, which affects the electron charge transfer process. As for example, TPA-N(CH₃)₂ rises up the LUMO level of the TPA- N(CH₃)₂ by an amount of 0.09 eV thereby increasing the electron injection rate from photo-excited dye to the TiO₂ surface. According to the Marcus theory of electron injection, which states that the larger the value of ΔG injects the faster the rate of electron injection. It is worthy to mention here that this assumption is valid as long as the injection is restricted to energy levels close to the conduction band edge, and that the density of the acceptor states in this energy range remains constant [49]. It is clearly indicated from Table 2 that the LUMOs of all dye molecules lie over the ECB of TiO₂ and the HOMO are situated below the redox potential of I₃⁻/I⁻ electrolyte (-4.80 eV). Thus values, it can be stated that all of them possesses a positive response to electron charge transfer and regeneration related to photo-oxidation process. Fig. 4 displays the relative energy levels of design dyes with reference to the conduction band of TiO₂ surface and triiodide /iodide as the redox couple. The figure depicts that TPA-N(CH₃)₂ is expected to show the fastest electron transfer among the dyes. Our prediction is also supported by greater charge separation between the HOMO and LUMO of this specified dye as could be found in Fig. 3.

3.4 Non-Linear Optical Properties

We have calculated the static dipole moment (μ), mean polarizability (α_0), polarizability anisotropy ($\Delta\alpha$), static first hyperpolarizability (β) and second hyperpolarizability (γ) at the ground state for design dye molecules. Design molecules were calculated using the formulas as [50-54]

$$\mu_{tot} = \sqrt{(\mu_x^2 + \mu_y^2 + \mu_z^2)} \quad (2)$$

$$\alpha_0 = \frac{(\alpha_{xx} + \alpha_{yy} + \alpha_{zz})}{3} \quad (3)$$

$$\Delta\alpha = \frac{1}{\sqrt{2}} \left[(\alpha_{xx} + \alpha_{yy})^2 + (\alpha_{zz} + \alpha_{xx})^2 + 6\alpha_{xx}^2 \right] \quad (4)$$

$$\beta = \left[(\beta_{xxx} + \beta_{yyy} + \beta_{zzz})^2 + (\beta_{xxy} + \beta_{yyx} + \beta_{zzz})^2 + (\beta_{xxz} + \beta_{zyy} + \beta_{zzz})^2 \right]^{1/2} \quad (5)$$

$$\gamma = \frac{1}{5} \left[(\gamma_{xxxx} + \gamma_{yyyy} + \gamma_{zzzz}) + 2(\gamma_{xxxx} + \gamma_{yyyy} + \gamma_{zzzz}) \right] \quad (6)$$

Where α_{xx} , α_{yy} and α_{zz} is the polarizability tensor components, β_{xxx} , β_{yyy} , β_{zzz} , β_{xxy} , β_{yyx} , β_{yzz} , β_{xxz} , β_{zyy} , β_{zzz} and γ_{xxxx} , γ_{yyyy} , γ_{zzzz} the first order and second order tensor components, respectively. The calculated values were summarized in Table 3. The $-\text{N}(\text{CH}_3)_2$ substituted TPA- $\text{N}(\text{CH}_3)_2$ molecule static polarizability has 3.73×10^{-23} e. s. u. The static polarizability of C206 has 4.98×10^{-23} e.s.u. The static polarizability is directly proportional to the dipole moment [55]. However, from Table 3 it can be seen that the value of OC_2H_5 substituted TPA- OC_2H_5 molecule has 3.82×10^{-23} e.s.u.

The first hyperpolarizability is inversely proportional to the transition energy. Accordingly, the TPA- $\text{N}(\text{CH}_3)_2$ substituted molecule with minimum transition energy (2.15 eV obtained from TD-DFT calculation) exhibits the maximum value of 2.01×10^{-28} e.s.u. The second order hyperpolarizability was calculated using the equation (6) and table 3 has shown second order hyperpolarizability results. Among the five dye molecules, more efficient second order hyperpolarizability values obtained in C206 dye molecules. The above results were depending on the donor, acceptor, π -bridge and functional group substitutions. Higher values of dipole moment, first and second-order hyperpolarizabilities were important for active NLO performance. The present results clearly include that the TPA- $\text{N}(\text{CH}_3)_2$ dye molecule particularly can be used in NLO applications.

3.5 Absorption Properties

Based on the optimized molecular structures with B3LYP/6-311++G(d,p) method, the UV-Vis spectra of the dyes using TD-DFT calculations in chloroform with B3LYP hybrid functional taking the lowest 20 spin-allowed singlet-singlet transitions were calculated. Before computing the absorption spectra, the dipole moment values of the individual dye systems have been analyzed and are tabulated in Table 3. The highest dipole moment values

indicate that all the dyes are polar molecules. Table 4 also provides the vertical excitation energy (E^*), oscillator strength (f), and the light harvesting efficiency (LHE) of the parent and the substituted dyes. All the dyes show a broad UV-Vis spectra whose tails enter into the chloroform IR region rendering a broad light harvesting power. In Fig. 5 shows the computed UV-Visible spectra of some representative dyes in chloroform solvent. It is clear from the figure that, all the dyes show two absorption peaks, one in the visible region (around 600 nm) and another in the far-infrared region; the corresponding values of maximum absorption wavelength (λ_{\max}) for all the dyes are given in Table 4. For the dye TPA- $N(CH_3)_2$, the $\lambda_{\max}=576$ nm is assigned to be mainly due to HOMO \rightarrow LUMO transition, whereas the second broad absorption peak at 432 nm corresponds to HOMO-3 \rightarrow LUMO transition. On the other hand, for another two dyes, the HOMO-LUMO transition becomes the highest intensity peaks, which can be interpreted by the more co-planar nature of TPA and TPA-SCH₃ than that of C206 molecules. Table 4 Indicates that there is a pronounced effect on the λ_{\max} , oscillator strength and hence LHE with substitution compared with C206 dye [56]. For most of the substituted dye molecule systems, there is increased oscillator strength than the corresponding main dye system that is C206. The LHE factor determines the efficiency of DSSC.

Highest oscillator strength and hence high LHE is found for TPA. λ_{\max} is found to be the highest for TPA- $N(CH_3)_2$ dye molecule which gives LHE is 0.8433. From the calculated data, it can also be inferred that in the case of electron donating- $N(CH_3)_2$ substituent there is always a higher value of λ_{\max} , oscillator strength, and LHE as compared to the corresponding other substituted dyes. The overall efficiency (η) of the DSSC can be computed from the open circuit voltage (V_{OC}), short-circuit current density (J_{SC}), the fill factor (FF) and the intensity of incident solar light (P_{IN}) as expressed in equation (1). The values of J_{SC} , V_{OC} , and FF can be obtained from the current-voltage characteristics in the illuminated condition. Only analytical relationship between V_{OC} and E_{LUMO} of the dye may be expressed as:

$$eV_{OC}=E_{LUMO}-E_{CB} \quad (7)$$

Where E_{CB} is the conduction band energy of the semiconductor surface. It induces that the higher the value of E_{LUMO} , larger is that for V_{OC} . The computed values of eV_{OC} for the dyes are given in Table 4 which depicts that the V_{OC} is maximum for TPA- $N(CH_3)_2$.

4. Conclusions

In the present study, different structural modifications have been optimized for the photovoltaic and NLO properties of the TPA-based dye molecules. The theoretical calculation to gain insights into the geometric and electronic structures of the dyes were discussed and compared with the experimental data. All the dyes were found to fulfill the criteria for using efficient sensitizers in DSSCs. The substitutes are found to have a huge effect on the optoelectronic properties of the dyes. Substitution of TPA-N(CH₃)₂ group emerged to be most successful. In all the dyes TPA-N(CH₃)₂ substitutions resulted in a decrease of open circuit voltage ($eV_{oc} = 0.8$ eV), while significant by a decrease in band gap (2.15 eV) and remarkably increased excitation wavelength (576 nm). So, it can be concluded that substitution of TPA-N(CH₃)₂ group is suitable to meet the needs of efficient dye. C206 dye has the highest second order hyperpolarizability (7.089×10^{-28} e.s.u) compared to the other dyes. While, the substitution of the TPA-OC₂H₅ group has not been much successful. Unsubstitution of TPA resulted all along positively in the case of C206 leading to a decrease in band gap energy and increase in oscillator strength consequently, while the LHE value along with a significant decrease in open circuit voltage ($eV_{oc} = 1.06$ eV). Dyes, viz TPA-SCH₃ and TPA-OC₂H₅ give mixed results. In both cases, it lowers band gap energy and increases the open circuit voltage but decreases the oscillator strength. The guideline provided by these studies would be very effective for identifying the NLO properties and fabrication of the photovoltaic devices.

Acknowledgements

The authors are thankful to the learned referees for their useful and critical comments, which are to be, improved the quality of the manuscript. One of the authors M. Prakasam acknowledges Periyar University for financial support in the form of University Research Fellow (URF).

Table 1 Geometric Parameters of Some Selected Dihedral Angles of the Optimized Dyes

Dye	Degree	TPA	Degree	TPA- N(CH ₃) ₂	Degree	TPA- SCH ₃	Degree	TPA- OC ₂ H ₅	Degree
C50- C49- C42- H15	178.37	H41- C11- C10- H40	- 179.60	H60- C49- C42- H15	- 179.67	S59- C17- C16- H44	178.55	O51- C17- C16- H44	- 179.64
C50- C49- C42- H16	- 177.39	H41- C11- C12- H42	- 179.72	H60- C17- C18- H48	- 179.96	S59- C17- C16- H45	- 179.70	O51- C17- C18- H45	- 179.79
C71- C70- C11- H39	- 177.94	H46- C17- C16- H45	- 179.71	H51- C11- C12- H41	- 179.99	S60- C11- C12- H41	- 179.63	O59- C11- C12- H41	- 179.76
C71- C70- C10- H38	178.92	H46- C17- C18- H47	- 179.61	H51- C11- C12- H41	- 179.56	S60- C11- C10- H40	178.46	O59- C11- C18- H40	- 179.62

Table 2 Frontier molecular orbital energy levels (with respect to vacuum) and the Corresponding optical gap of the different dyes in B3LYP and wB97XD method

Dye/Method	B3LYP			wB97XD		
	HOMO (in eV)	LUMO (in eV)	Band Gap (in eV)	HOMO (in eV)	LUMO (in eV)	Band Gap (in eV)
C206	-5.30	-2.88	2.42	-7.02	-1.28	5.74
TPA	-5.19	-2.94	2.25	-6.95	-1.35	5.6
TPA-N(CH ₃) ₂	-5.10	-3.20	2.10	-6.74	-1.16	5.58
TPA-SCH ₃	-5.44	-2.93	2.51	-7.20	-1.32	5.88
TPA-OC ₂ H ₅	-5.91	-2.72	3.19	-6.25	-1.06	5.19

Table 3 The Dipole Moment, Static Polarizability, First and Second Order Hyperpolarizability of Dyes Studied at B3LYP/6-311+G (d,p) Level of Theory

Dye	Dipole Debye	Polarizability $\times 10^{-23}$ e.s.u	First order Hyperpolarizability $\times 10^{-29}$ e.s.u	Second order Hyperpolarizability $\times 10^{-28}$ e.s.u
C206	4.79	4.98	1.25	7.089
TPA	14.75	3.14	1.43	3.080
TPA-N(CH ₃) ₂	16.57	3.73	2.01	4.188
TPA-SCH ₃	9.97	4.06	1.33	4.285
TPA-OC ₂ H ₅	14.33	3.82	1.88	4.282

Table 4 Vertical Excitation Energy, Oscillator Strength and Photovoltaic Parameters of the Different Dyes

Dye	E* (eV)	λ_{max} (nm)	Oscillator Strength (f)	LHE	eV_{oc} (eV)
C206*	2.44	508	0.6834	0.7926	1.12
TPA	2.65	468	1.3948	0.9597	1.06
TPA-N(CH ₃) ₂	2.15	576	0.8052	0.8433	0.80
TPA-SCH ₃	2.64	470	0.8095	0.8849	1.07
TPA-OC ₂ H ₅	2.38	521	0.9716	0.8932	1.28

*ref. [56]

References

1. B. O' Reagan and M. Grätzel, *Nature.*, 1991, **353**, 737-740.
2. M. Grätzel, *Nature.*, 2001, **414**, 338-344.
3. S. Lyu, Y. Farré, L. Ducasse, Y. Pellegrin, T. Toupance, C. Olivier, F. Odobel, *RSC Adv.*, 2016, **6**, 19928-19936.

4. S. Mathew, A. Yella, P. Gao, R. Humphry-Baker, B.F. E. Curchod, N. Ashari-Astani, I. Tavernelli, U. Rothlisberger, Md. K. Nazeeruddin and M.K. Gratzel, *Nat. Chem.*, 2014, **6**, 242-247.
5. C.-Y. Chen, M. K. Wang, J.-Y. Li, N. Pootrakulchote, L. Alibabaei, C. H. Ngoc-le, J. D. Decoppet, J. H. Tsai, C. Graetzel and C. G. Wu, et al., *ACS Nano.*, 2009, **3**, 3103-3109.
6. Z. Yang, C. Shao, D. Cao, *RSC Adv.*, 2015, **5**, 22892-22898.
7. H. Li, Y. Li, M. Chen, *RSC Adv.*, 2014, **4**, 57916-57922.
8. Y. Saito, N. Fukuri, R. Senadeera, T. Kitamura, Y. Wada and S. Yanagida, *Electrochem. Commun.*, 2004, **6**, 71-74.
9. J. B. Asbury, R. J. Ellingson, H. N. Ghosh, S. Ferrere, J. Nozik and T. Lian, *J. Phys. Chem. B.*, 1993, **103**, 3110-3119.
10. J. H. Werner, Second and Third Generation Photovoltaics- Dreams and Reality, in *Advances in Solid State Physics*, ed.B. Kramer, Springer, Berlin Heidelberg, Germany, 2004, **44**, 172-172.
11. R. Argazzi, G. Larramona, C. Contado and C. A. Bignozzi, *Photochem. Photobio A.*, 2004, **164**, 15-21
12. Y. Koyama, T. Miki, X.-F. Wang and H. Nagaie, *Int. J. Mol. Sci.*, 2009, **10**, 45754-4622.
13. P. Senthilkumar, C. Nithya, P.M. Anbarasan, *Spectrochimica Acta Part A: Molecular and Biomolecular Spectroscopy.*, 2014, **122**, 15-21.
14. T. Kitamura, M. Ikeda, K. Shigaki, T. Inoue, N. A. Anderson, X. Ai, T. Q. Lian and S. Yanagida, *Chem. Mater.*, 2004, **16**, 1806-1812.
15. G. Yu, J. Gao, J. C. Hummelen, F. Wudl and A. Heeger, *Science*, 1995, **270**, 1789-1791.
16. Y. J. Cheng, S. H. Yang and C. S. Hsu, *Chem. Rev.*, 2009, **109**, 5868-5923.
17. T.-Y. Chu, J. Lu, S. Beaupre', Y. Zhang, J.-R. Pouliot, S. Wakim, J. Zhou, M. Leclerc, Z. Li, J. Ding and Y. Tao, *J. Am. Chem. Soc.*, 2011 **133**, 4250-4253.
18. D. Cahen, G. Hodes, M. Graetzel, J. F. Guillermales and J. Riess, *J. Phys. Chem. B.*, 2000, **104**, 2053-2059.
19. N.N. Ghosh, A. Chakraborty, S. Pal, A. Pramanik, P. Sarkar, *Phys. Chem. Chem. Phys.*, 2014, **16**, 25280-25287.
20. J. B. Asbury, Y. Q. Wang, E. Hao, H. N. Ghosh and T. Lian, *Res. Chem. Intermed.*, 2001, **27**, 393-406.

21. W. Sang-aroon, S. Saekow and V. Amornkitbamrung, *Photochem. Photobio., A*, 2012, **236**, 35-42
22. J. Preat, C. Michaux, D. Jacquemin and E. A. Perpete, *J. Phys. Chem. C.*, 2009, **113**, 16821-16833.
23. C. J. Brabec, C. Winder, N. S. Sariciftci, J. C. Hummelen, Dhanabalan, P. A. van Hal and R. A. J. Janssen, *Adv. Funct. Mater.*, 2002, **12**, 709-712.
24. J. J. M. Halls, J. Cornil, D. A. dos Santos, R. Silbey, D.-H. Hwang, A. B. Holmes, J. L. Brdas and R. H. Friend, *Phys. Rev. B: Condens. Matter Mater. Phys.*, 1999, **60**, 5721-5757.
25. W. Zhongquan, J. Chunyang, W. Yan Wanga, Y. Xiaojun, *RSC Adv.*, 2015, **5**, 50813-50820
26. Hagfeldt, G. Boschloo, L. Sun, L. Kloo and H. Pettersson, *Chem. Rev.*, 2010, **110**, 6595-6663.
27. A. Mishra, M. K. R. Fischer and P. Buerle, *Angew. Chem., Int. Ed.* 2009, **48**, 2474-2499.
28. R. Kroon, M. Lenes, J. C. Hummelene, P. W. M. Blom and B. De Boe, *Polym. Rev.*, 2008, **48**, 531-582.
29. Handbook of Organic Conductive Molecules and Polymers, ed. H. S. Nalwa, John Wiley and Sons, 1999.
30. Z. Wan, C. Jia, Y. Duan, L. Zhou, J. Zhang, Y. Lin, Y. Shi, *RSC Adv.*, 2012, **2**, 4507-4514.
31. T. Suresh, R.K. Chitumalla, N.T. Hai, J. Jang, T.J. Lee, J.H. Kim, *RSC Adv.*, 2016, **6**, 26559-26567
32. M. de Wergifosse, B. Champagne, S. Ito, K. Fukuda M. Nakano, *Phys. Chem. Chem. Phys.*, 2016, **18**, 6420-6429
33. E. Lim, B.-J. Jung, H.-K. Shim, T. Taguchi, B. Noda, T. Kambayashi, T. Mori, K. Ishikawa, H. Takezoe and L.-M. Do, *Org. Electron.*, 2006, **7**, 121-131.
34. Z. Ning and H. Tian, *Chem. Commun.*, 2009, **37**, 5483-5495.
35. Z. Ning, Q. Zhang, W. Wu and H. Tian, *J. Org. Chem.*, 2008, **733**, 3791-3797.
36. D. Liu, R. W. Fessenden, G. L. Hug and P. V. Kamat, *J. Phys. Chem. B.*, 1997, **101**, 2582-2585.
37. A. Mahmood, S.D. Khan, U. A. Rana, M. R. S. A. Janjua, M. H. Tahir, M. F. Nazar and Y. Song, *J. Phy. Org. Chem.*, 2015, **28**, 418-422.
38. Y. Zhao, K. Jiang, W. Xu, D. Zhu, *Tetrahedron.*, 2012, **68**, 9113-9118.

39. M. J. Frisch, G. W. Trucks, H. B. Schlegel, G. E. Scuseria, A. Robb, J. R. Cheeseman, G. Scalmani, V. Barone, B. Mennucci and G. A. Petersson, et al., Gaussian 09, revision C.04, Gaussian, Inc., Wallingford, CT, 2009.
40. R. Ditchfield, W. J. Hehre and J. A. Pople, *J. Chem. Phys.*, 1971, **54**, 724-728.
41. A. D. Beche, *J. Chem. Phys.*, 1993, **98**, 5648-5652.
42. S. Grimme, A. Jens, E. Stephan, K. Helge Krieg, *J Chem Phys.*, 2010, 132, 154104.
43. M. D. Liptak and G. C. Shields, *Int. J. Quantum Chem.*, 2005, **105**, 580-587.
44. S. Miertus and J. Tomasi, *Chem. Phys.* 1982, **65**, 239-245.
45. S. Md. Pratik and A. Datta, *Phys. Chem. Chem. Phys.*, 2013, **15**, 18471-18481.
46. J. Feng, Y. Jiao, W. Ma, Md. K. Nazeeruddin, M. Grätzel and S. Meng, *J. Phys. Chem. C.*, 2013, **117**, 3772-3778.
47. K. Ozawa, M. Emori, S. Yamamoto, R. Yukawa, S. Yamamoto, R. Hobara, K. Fujikawa, H. Sakama and I. Matsuda, *J. Phys. Chem. Lett.*, 2014, **5**, 1953-1957.
48. R. Chen, X. Yang, H. Tian and L. Sun, *Photochem. Photobio A.*, 2007, **189**, 295-300.
49. R. A. Marcus and N. Sutin, *Biochim. Biophys. Acta*, 1985, **811**, 265-322.
50. W. Zhongquan, J. Chunyang, W. Yan Wanga, Y. Xiaojun, *RSC Adv.*, 2015, **5**, 50813-50820
51. K. Lanke and N. Sekar, *J Fluoresc.*, 2015, **25**, 1469-1480.
52. P. Senthilkumar, C. Nithya, P. M. Anbarasan, *Spectrochimica Acta Part A: Molecular and Biomolecular Spectroscopy.*, 2014, **122**, 15-21.
53. P. Senthilkumar, C. Nithya, P. M. Anbarasan, *J Mol Model.*, 2013, **19**, 4561-4573.
54. P. Senthilkumar, C. Nithya, P. M. Anbarasan, *Spectrochimica Acta Part A: Molecular and Biomolecular Spectroscopy.*, 2014, **117**, 181-185.
55. M. R. S. A. Janjua, M. U. Khan, B. Bashir, M. A. Iqbal, Y. Song, S. A. R. Naqvi and Z. A. Khan, *Comput. Theor. Chem.*, 2012, **994**, 34-40.
56. G. Zhang, H. Bala, Y. Cheng, D. Shi, X. Lv, Q. Yu and P. Wang, *Chem. Commun.*, 2009, **16**, 2198-2200.

Figure Captions

- Fig. 1** Chemical structure of TPA based dye sensitizers
- Fig. 2** Optimized ground state geometries of the dyes in the gas phase obtained at the B3LYP/6-311++G(d,p)
- Fig. 3** The frontier molecular orbital's of HOMO (left) and LUMO (right)
- Fig. 4** Schematic energy level diagrams of the dyes, CB of TiO₂ and electrolyte (I⁻/I₃⁻)
- Fig. 5** Computed UV-Visible spectra of some representative dyes in chloroform solvent

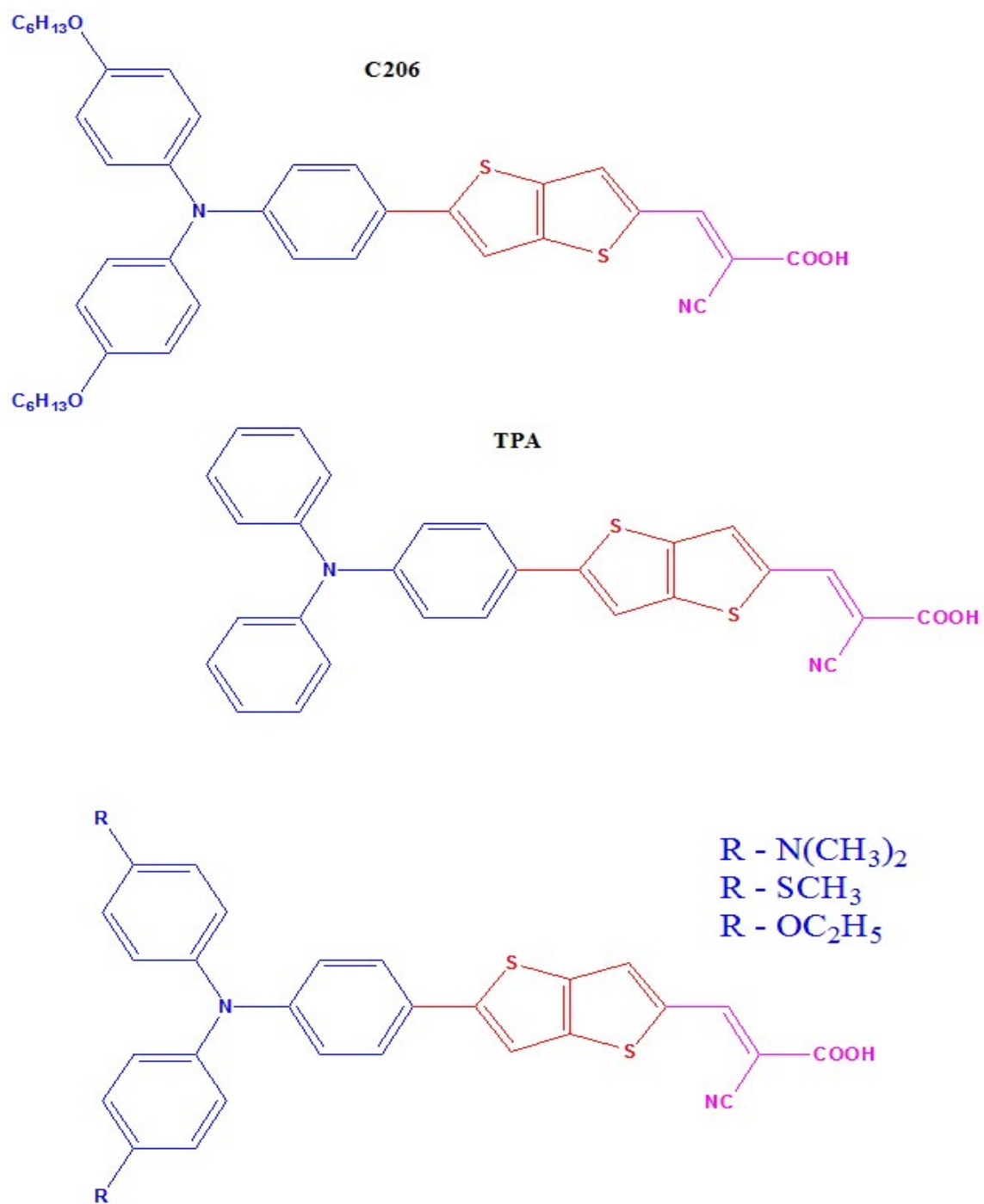


Fig. 1

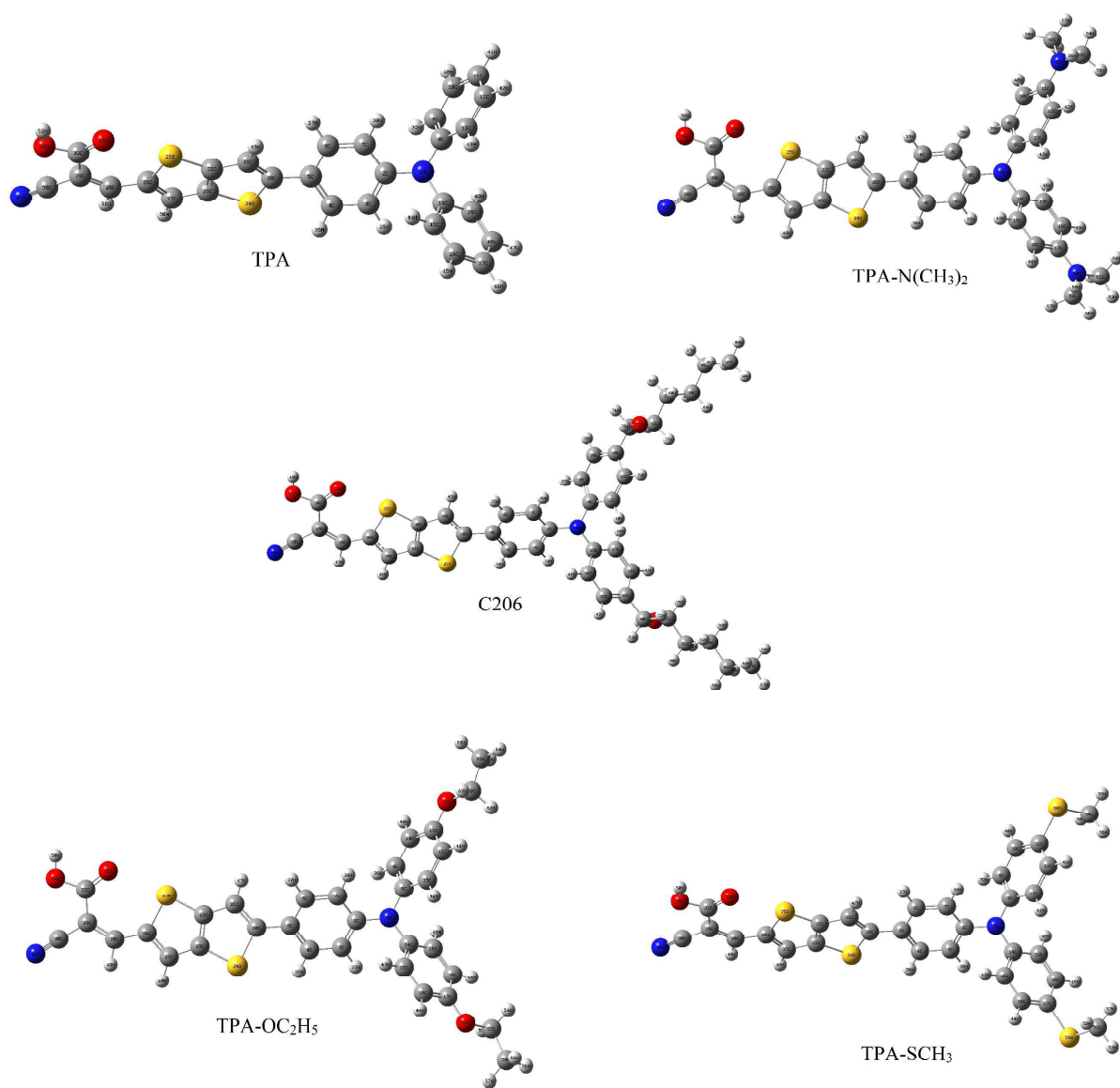


Fig. 2

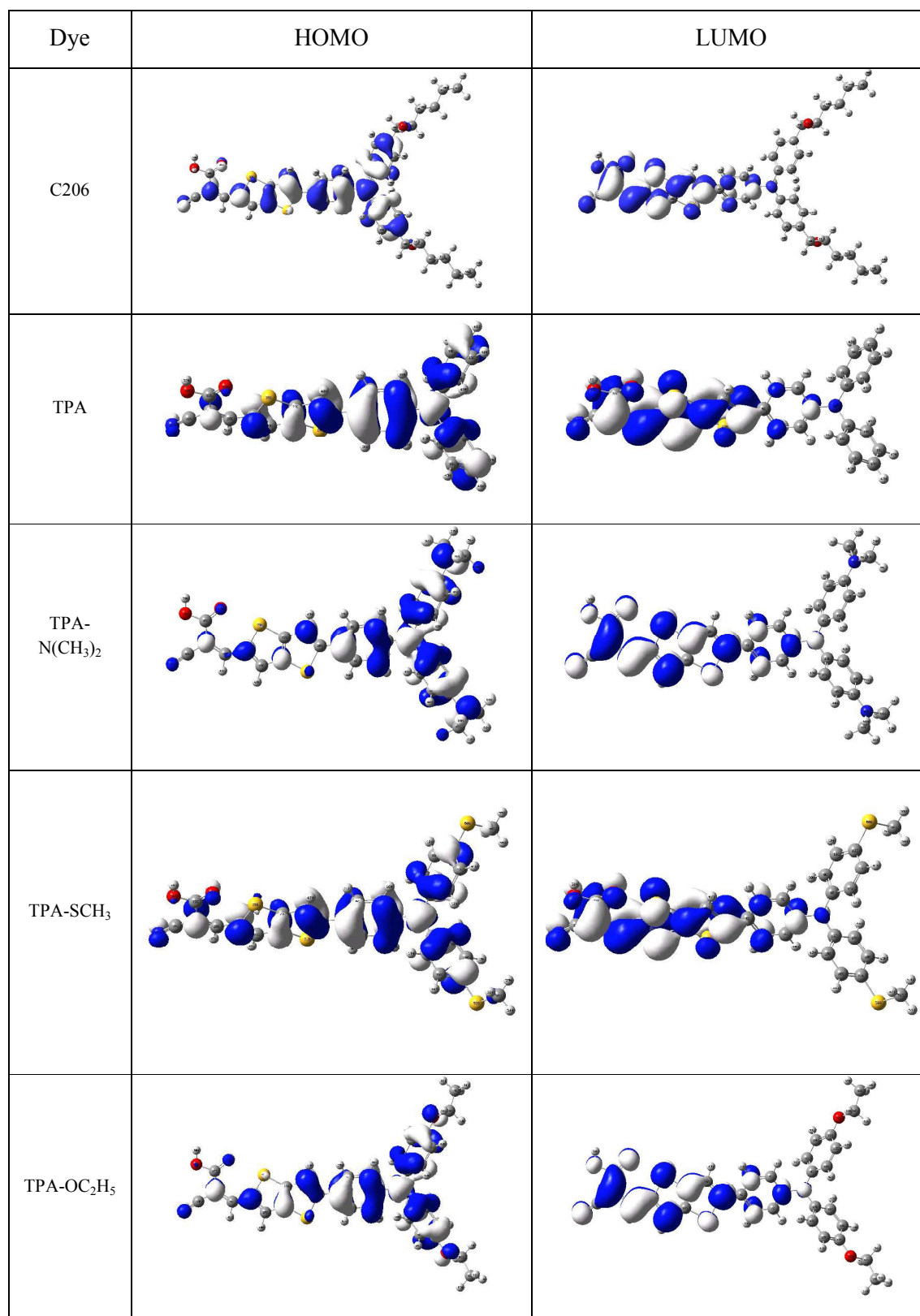


Fig. 3

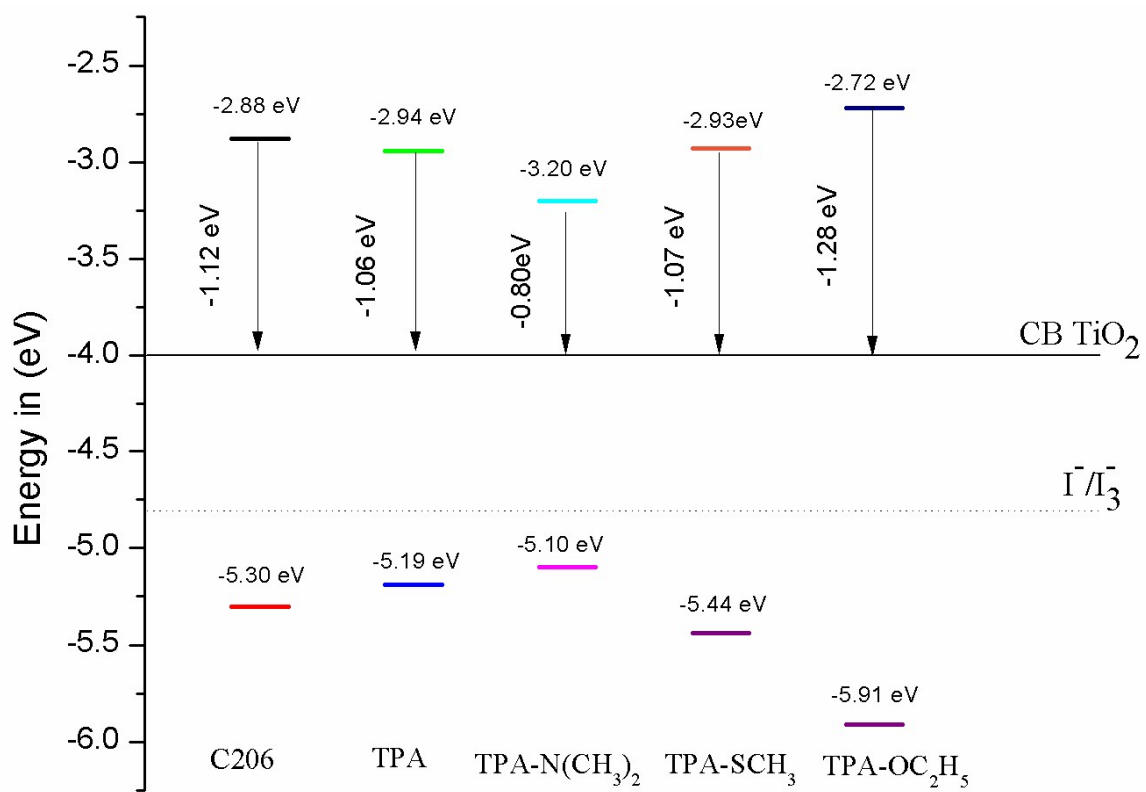


Fig. 4

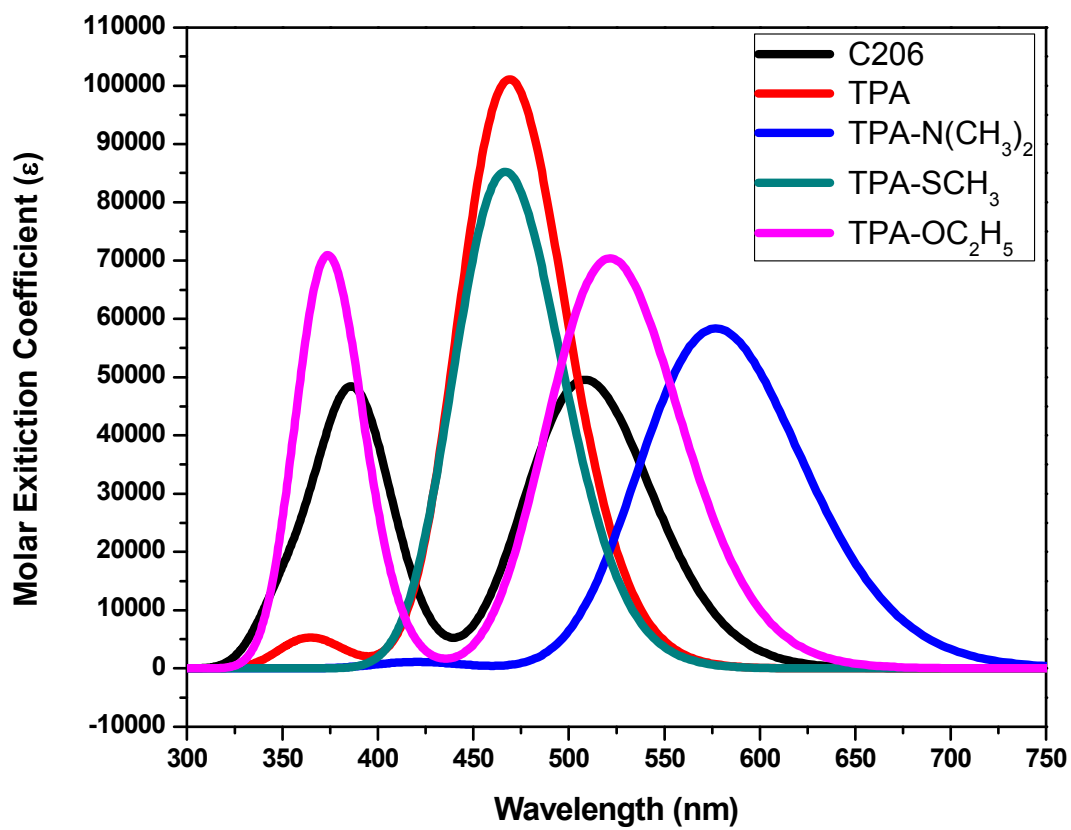


Fig. 5